Research Article | Vol. 24, No. 25 | 12 Dec 2016 | OPTICS EXPRESS 29060

Optics EXPRESS

Comparison of attosecond streaking and RABBITT

L. CATTANEO,[1,*] J. VOS,[1] M. LUCCHINI,[1] L. GALLMANN,[1,2] C. CIRELLI,[1] AND U. KELLER[1]

[1]*Physics Department, ETH Zurich, 8093 Zurich, Switzerland*
[2]*Institute of Applied Physics, University of Bern, 3012 Bern, Switzerland*
[*]*claura@phys.ethz.ch*

Abstract: Recent progress in the generation of ultra-short laser pulses has enabled the measurement of photoionization time delays with attosecond precision. For single photoemission time delays the most common techniques are based on attosecond streaking and the reconstruction of attosecond beating by interference of two-photon transitions (RABBITT). These are pump-probe techniques employing an extreme-ultraviolet (XUV) single attosecond pump pulse for streaking or an attosecond pump pulse train for RABBITT, and a phase-locked infrared (IR) probe pulse. These techniques can only extract *relative* timing information between electrons originating from different initial states within the same atom or different atoms. Here we address the question whether the two techniques give identical timing information. We present a complete study, supported by both experiments and simulations, comparing these two techniques for the measurement of the photoemission time delay difference between valence electrons emitted from the Ne 2p and Ar 3p ground states. We highlight not only the differences and similarities between the two techniques, but also critically investigate the reliability of the methods used to extract the timing information.

OCIS codes: (020.0020) Atomic and molecular physics; (320.7100) Ultrafast measurements.

References and links

1. P. Eckle, A. N. Pfeiffer, C. Cirelli, A. Staudte, R. Dörner, H. G. Muller, M. Büttiker, and U. Keller, "Attosecond ionization and tunneling delay time measurements in helium," Science **322**(5907), 1525–1529 (2008).
2. A. S. Landsman, M. Weger, J. Maurer, R. Boge, A. Ludwig, S. Heuser, C. Cirelli, L. Gallmann, and U. Keller, "Ultrafast resolution of tunneling delay time," Optica **1**(5), 343–349 (2014).
3. M. Schultze, M. Fiess, N. Karpowicz, J. Gagnon, M. Korbman, M. Hofstetter, S. Neppl, A. L. Cavalieri, Y. Komninos, T. Mercouris, C. A. Nicolaides, R. Pazourek, S. Nagele, J. Feist, J. Burgdörfer, A. M. Azzeer, R. Ernstorfer, R. Kienberger, U. Kleineberg, E. Goulielmakis, F. Krausz, and V. S. Yakovlev, "Delay in photoemission," Science **328**(5986), 1658–1662 (2010).
4. K. Klünder, J. M. Dahlström, M. Gisselbrecht, T. Fordell, M. Swoboda, D. Guénot, P. Johnsson, J. Caillat, J. Mauritsson, A. Maquet, R. Taïeb, and A. L'Huillier, "Probing Single-Photon Ionization on the Attosecond Time Scale," Phys. Rev. Lett. **106**(14), 143002 (2011).
5. M. Sabbar, S. Heuser, R. Boge, M. Lucchini, T. Carette, E. Lindroth, L. Gallmann, C. Cirelli, and U. Keller, "Resonance effects in photoemission time delays," Phys. Rev. Lett. **115**(13), 133001 (2015).
6. R. Locher, L. Castiglioni, M. Lucchini, M. Greif, L. Gallmann, J. Osterwalder, M. Hengsberger, and U. Keller, "Energy-dependent photoemission delays from noble metal surfaces by attosecond interferometry," Optica **2**(5), 405–410 (2015).
7. S. Haessler, B. Fabre, J. Higuet, J. Caillat, T. Ruchon, P. Breger, B. Carré, E. Constant, A. Maquet, E. Mével, P. Salières, R. Taïeb, and Y. Mairesse, "Phase-resolved attosecond near-threshold photoionization of molecular nitrogen," Phys. Rev. A **80**(1), 011404 (2009).
8. A. L. Cavalieri, N. Müller, T. Uphues, V. S. Yakovlev, A. Baltuška, B. Horvath, B. Schmidt, L. Blümel, R. Holzwarth, S. Hendel, M. Drescher, U. Kleineberg, P. M. Echenique, R. Kienberger, F. Krausz, and U. Heinzmann, "Attosecond spectroscopy in condensed matter," Nature **449**(7165), 1029–1032 (2007).
9. J. Itatani, F. Quéré, G. L. Yudin, M. Y. Ivanov, F. Krausz, and P. B. Corkum, "Attosecond streak camera," Phys. Rev. Lett. **88**(17), 173903 (2002).
10. M. Hentschel, R. Kienberger, C. Spielmann, G. A. Reider, N. Milosevic, T. Brabec, P. Corkum, U. Heinzmann, M. Drescher, and F. Krausz, "Attosecond metrology," Nature **414**(6863), 509–513 (2001).
11. P. M. Paul, E. S. Toma, P. Breger, G. Mullot, F. Augé, P. Balcou, H. G. Muller, and P. Agostini, "Observation of a train of attosecond pulses from high harmonic generation," Science **292**(5522), 1689–1692 (2001).

#279664 http://dx.doi.org/10.1364/OE.24.029066
Journal © 2016 Received 27 Oct 2016; revised 2 Dec 2016; accepted 5 Dec 2016; published 7 Dec 2016

Optics EXPRESS

12. H. G. Muller, "Reconstruction of attosecond harmonic beating by interference of two-photon transitions," Appl. Phys. B **74**(S1), S17–S21 (2002).
13. C. Palatchi, J. M. Dahlström, A. S. Kheifets, I. A. Ivanov, D. M. Canaday, P. Agostini, and L. F. DiMauro, "Atomic delay in helium, neon, argon and krypton," J. Phys. B: At. Mol. Opt. **47**(24), 245003 (2014).
14. D. Guenot, D. Kroon, E. Balogh, E. W. Larsen, M. Kotur, M. Miranda, T. Fordell, P. Johnsson, J. Mauritsson, M. Gisselbrecht, K. Varjù, C. L. Arnold, T. Carette, A. S. Kheifets, E. Lindroth, A. LHuillier, and J. M. Dahlström, "Measurements of relative photoemission time delays in noble gas atoms," J. Phys. B **47**(24), 245602 (2014).
15. C. Cirelli, M. Sabbar, S. Heuser, R. Boge, M. Lucchini, L. Gallmann, and U. Keller, "Energy-dependent photoemission time delays of noble gas atoms using coincidence attosecond streaking," IEEE J. Sel. Top. Quantum Electron. **21**(5), 1–7 (2015).
16. M. Lucchini, A. Ludwig, L. Kasmi, L. Gallmann, and U. Keller, "Semi-classical approach to compute RABBITT traces in multi-dimensional complex field distributions," Opt. Express **23**(7), 8867–8879 (2015).
17. R. Pazourek, S. Nagele, and J. Burgdörfer, "Attosecond chronoscopy of photoemission," Rev. Mod. Phys. **87**(3), 765–802 (2015).
18. Y. Mairesse and F. Quéré, "Frequency-resolved optical gating for complete reconstruction of attosecond bursts," Phys. Rev. A **71**(1), 011401 (2005).
19. J. Gagnon and V. S. Yakovlev, "The robustness of attosecond streaking measurements," Opt. Express **17**(20), 17678–17693 (2009).
20. H. Wei, T. Morishita, and C. D. Lin, "Critical evaluation of attosecond time delays retrieved from photoelectron streaking measurements," Phys. Rev. A **93**(5), 053412 (2016).
21. R. Dörner, V. Mergel, O. Jagutzki, L. Spielberger, J. Ullrich, R. Moshammer, and H. Schmidt-Böcking, "Cold Target Recoil Ion Momentum Spectroscopy: a 'momentum microscope' to view atomic collision dynamics," Phys. Rep. **330**(2-3), 95–192 (2000).
22. M. Sabbar, S. Heuser, R. Boge, M. Lucchini, L. Gallmann, C. Cirelli, and U. Keller, "Combining attosecond XUV pulses with coincidence spectroscopy," Rev. Sci. Instrum. **85**(10), 103113 (2014).
23. G. Sansone, E. Benedetti, F. Calegari, C. Vozzi, L. Avaldi, R. Flammini, L. Poletto, P. Villoresi, C. Altucci, R. Velotta, S. Stagira, S. De Silvestri, and M. Nisoli, "Isolated single-cycle attosecond pulses," Science **314**(5798), 443–446 (2006).
24. E. P. Wigner, "Lower Limit for the Energy Derivative of the Scattering Phase Shift," Phys. Rev. **98**(1), 145–147 (1955).
25. F. T. Smith, "Lifetime Matrix in Collision Theory," Phys. Rev. **118**(1), 349–356 (1960).
26. J. M. Dahlström, T. Carette, and E. Lindroth, "Diagrammatic approach to attosecond delays in photoionization," Phys. Rev. A **86**(6), 061402 (2012).
27. V. S. Yakovlev, J. Gagnon, N. Karpowicz, and F. Krausz, "Attosecond streaking enables the measurement of quantum phase," Phys. Rev. Lett. **105**(7), 073001 (2010).
28. M. Kitzler, N. Milosevic, A. Scrinzi, F. Krausz, and T. Brabec, "Quantum theory of attosecond XUV pulse measurement by laser dressed photoionization," Phys. Rev. Lett. **88**(17), 173904 (2002).
29. D. J. Kane, "Recent progress toward real-time measurement of ultrashort laser pulses," IEEE J. Quantum Electron. **35**(4), 421–431 (1999).
30. J. Gagnon, E. Goulielmakis, and V. S. Yakovlev, "The accurate FROG characterization of attosecond pulses from streaking measurements," Appl. Phys. B **92**(1), 25–32 (2008).
31. A. S. Kheifets, "Time delay in valence-shell photoionization of noble-gas atoms," Phys. Rev. A **87**(6), 063404 (2013).
32. T. Carette, J. M. Dahlström, L. Argenti, and E. Lindroth, "Multiconfigurational Hartree-Fock close-coupling ansatz: Application to the argon photoionization cross section and delays," Phys. Rev. A **87**(2), 023420 (2013).
33. S. B. Schoun, R. Chirla, J. Wheeler, C. Roedig, P. Agostini, L. F. DiMauro, K. J. Schafer, and M. B. Gaarde, "Attosecond pulse shaping around a Cooper minimum," Phys. Rev. Lett. **112**(15), 153001 (2014).
34. M. Kotur, D. Guénot, Á. Jiménez-Galán, D. Kroon, E. W. Larsen, M. Louisy, S. Bengtsson, M. Miranda, J. Mauritsson, C. L. Arnold, S. E. Canton, M. Gisselbrecht, T. Carette, J. M. Dahlström, E. Lindroth, A. Maquet, L. Argenti, F. Martín, and A. L'Huillier, "Spectral phase measurement of a Fano resonance using tunable attosecond pulses," Nat. Commun. **7**, 10566 (2016).
35. V. Gruson, L. Barreau, Á. Jiménez-Galan, F. Risoud, J. Caillat, A. Maquet, B. Carré, F. Lepetit, J.-F. Hergott, T. Ruchon, L. Argenti, R. Taïeb, F. Martín, and P. Salières, "Attosecond dynamics through a Fano resonance: Monitoring the birth of a photoelectron," Science **354**(6313), 734–738 (2016).
36. M. Chini, S. Gilbertson, S. D. Khan, and Z. Chang, "Characterizing ultrabroadband attosecond lasers," Opt. Express **18**(12), 13006–13016 (2010).
37. P. D. Keathley, S. Bhardwaj, J. Moses, G. Laurent, and F. X. Kärtner, "Volkov transform generalized projection algorithm for attosecond pulse characterization," New J. Phys. **18**(7), 073009 (2016).

1. Introduction

The possibility to investigate attosecond ionization time delays in atoms was demonstrated almost one decade ago with the first experiments in the strong field regime [1,2], where an atom was ionized with a photon energy much lower than the ionization potential. Single-

Optics EXPRESS

photon photoemission delays were measured shortly afterwards for the first time [3,4] using photon energies well above the target ionization potential. More recently such photoemission delays were also measured in more complex targets such as molecules [7] and condensed matter [6,8].

Currently, the most common techniques to investigate the single-photon photoemission time delay are based on either the attosecond energy streaking [9,10] or the reconstruction of attosecond beating by interference of two-photon transitions (RABBITT) [11,12]. Both techniques employ a pump-probe scheme, where an extreme-ultraviolet (XUV) pump pulse initiates electron dynamics and an infrared (IR) probe pulse interrogates the temporal evolution as the delay between pump and probe is varied. While the RABBITT technique uses an attosecond pulse train (APT) in combination with a less intense and typically longer IR pulse, attosecond streaking method uses a single attosecond pulse (SAP) as a pump and a more intense, few-cycle IR pulse as a probe.

In contrast to the strong-field ionization using the attoclock technique [1], we cannot self-calibrate the absolute time zero when the XUV pulse initiates the single photoemission dynamics. We therefore need to make a reference measurement and at the end we only have access to relative timing information of the photoionization process. For example, photoemission time delays between photoelectrons emitted from the 2p and 2s bound states of neon [3] or from the 3p and 3s bound states of argon [4] have been measured with both techniques. Recently, it has been demonstrated that relative timing information between electrons liberated from different target species or even spatially separated targets can be extracted [5,13–15]. Today the much improved understanding of the attosecond measurements of the photoemission time delays from noble gases allows us to use them as a reference for more complex targets, thus giving access to absolute time delays in single photoemission as well [6,16]. Even though theoretical studies performed in noble gases suggest that both the RABBITT and energy streaking technique should result in the same delays [17], a direct experimental comparison has not been demonstrated so far.

Here we compare and test the accuracy of the measured single-photon photoemission delays using both the RABBITT and attosecond energy streaking technique. Figure 1 shows the basic principle of the two techniques to obtain energy-dependent relative photoemission time delays between photoelectron wave packets from the Ne 2p and Ar 3p ground states extracted with RABBITT [Figs. 1(a) and 1(b)] and attosecond energy streaking [Figs. 1(c) and 1(d)]. Both RABBITT and streaking traces [Figs. 1(b) and 1(d)] are represented as a function of the XUV photon energies, which implies that we add the ionization potential (I_p) of the gas under test to the measured photoelectron energy.

The comparison between the streaking and RABBITT techniques in this paper addresses not only the experimental aspects, but also the data-processing methods used in both techniques to extract the photoemission time delay information.

In particular, this investigation is also motivated by earlier work dedicated to a critical analysis of the reliability of the frequency resolved optical gating for complete reconstruction of attosecond bursts (FROG-CRAB) method [18] to retrieve the spectral intensity and phase of the electron wave packet (EWP) measured by attosecond streaking [19,20]. Gagnon et al. [19] commented on the fact that the properties of an emitted EWP cannot be fully described by a single complex-valued time-dependent function since in reality an attosecond streaking trace is accumulated over many laser pulses, meaning that one spectrogram is an ensemble of EWPs. In addition, a single spectrogram shows an average of the spatio-temporal properties of the SAP, which are usually not uniform. They concluded that the reconstruction of a SAP is generally robust and mainly suffers when there is a significant smearing of the electron spectra due to either energy or pump-probe delay uncertainties which consequently overestimate the pulse bandwidth and shorten the retrieved pulse duration [19]. However, to extract relative group delays of few tens of attoseconds we require a correspondingly high group delay accuracy which is much more challenging than the original application of the

Optics EXPRESS

FROG-CRAB algorithm for single attosecond pulse characterization [20]. Therefore we need to address the reliability of the reconstruction algorithm again for time delays in the tens of attosecond regime. We present here a complete analysis, supported by both experimental data and simulations, in order to highlight advantages, drawbacks, as well as potential pitfalls in each technique with the intention to serve as a guideline for better accuracy in data interpretation.

2. Methods and Results

Our experiments are performed with a so-called AttoCOLTRIMS apparatus, which consists of a reaction microscope or Cold Target Recoil Ion Momentum Spectroscopy (COLTRIMS) allowing for full 3D-coincidence detection [21] combined with an attosecond front-end, providing SAPs and APTs with photon energies in the XUV spectral range [22]. This system can provide both APTs using typically 30-fs IR pulses and SAPs with compressed 6-fs IR pulses at a pulse repetition rate of 10 kHz. For this additional pulse compression we use spectral broadening in a Ne-filled hollow-core fiber and subsequent dispersion compensation with chirped mirrors [22]. We use the polarization gating technique [23] to confine the high harmonic generation (HHG) to one half-cycle of the IR field and thus obtain a SAP. For the SAP case, the retrieved attochirp is in the order of 0.0195 ± 0.006 fs^2. The APT or SAP provides the XUV pump pulse and is focused into the gas jet target that contains a mixture of argon and neon in equal amounts in order to simultaneously ionize both species under identical experimental conditions. The released photoelectrons, after interacting with the IR probe field, are detected in coincidence with their parent ions allowing for the recording of the photoelectron spectra as a function of the pump-probe delay for each species. For both methods, the XUV-pump and the IR-probe pulse are linearly polarized and propagate collinearly with parallel polarizations.

2.1 RABBITT

In the RABBITT experiments, the XUV-APT is phase-locked with the IR pulse. Consecutive attosecond pulses in the train are separated by half an optical cycle of the generating IR pulse.

Optics EXPRESS

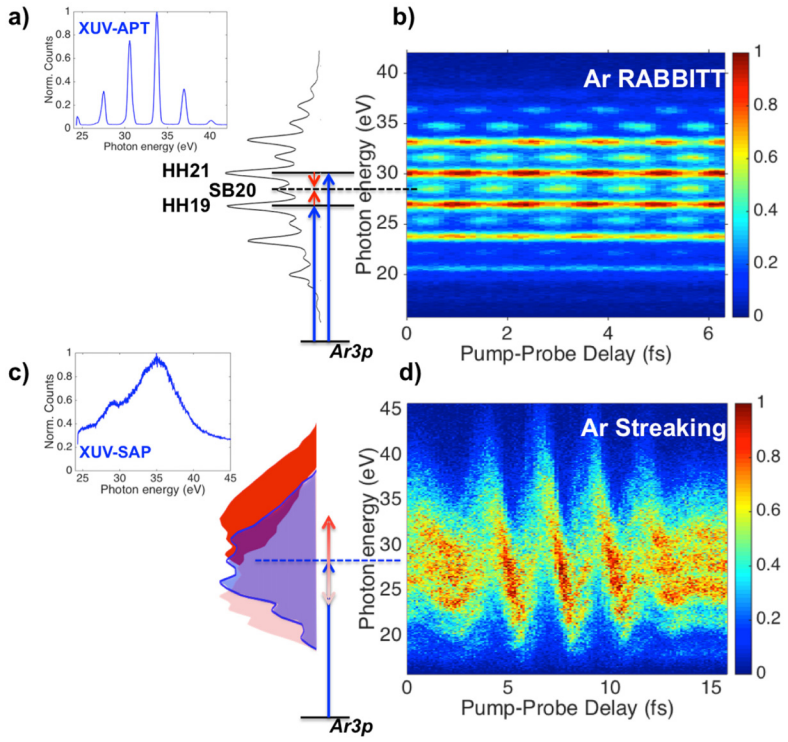

Fig. 1. a) Schematic view of the processes underlying a RABBITT measurement: the black solid curve represents the photoelectron spectrum generated by the interaction between Ar atoms and the pump-probe beams: the XUV-APT (spectrum in the top inset, blue solid curve) and the IR. The blue arrows indicate two transitions, both from the Ar 3p ground state to the continuum via absorption of an XUV photon belonging to either the 19th high-order harmonic (HH) or the 21st. In the presence of the IR field the 20th sideband (SB) will be populated via absorption of one IR photon from HH 19 or by emission of one IR photon from HH 21 (red arrows). Recording the electron spectra for different XUV-IR delays leads to a typical spectrogram shown in b). c) Represents the continuous distribution of photoelectrons (blue shaded area) produced by interaction of a XUV-SAP (spectrum in the inset, solid blue curve) with Ar atoms. If an additional IR field is present, the full spectrum shifts proportional to the vector potential of the IR field (pink/red areas). By recording the electron spectra as a function of the pump-probe delay we obtain a streaking trace as shown in d).

This XUV-APT corresponds to a frequency comb of high-order harmonics (HHs) separated by $2\omega_{IR}$ (ω_{IR} is the IR angular frequency), in our case centered at 35 eV (see the inset in Fig. 1(a)). When focused onto the cold Ar/Ne gas jet, it ionizes electrons into the continuum at photoelectron energies corresponding to the difference between the HH photon energies and the Ar or Ne ionization potentials (I_{pAr} = 15.76 eV and I_{pNe} = 21.56 eV). In the presence of a moderately intense IR-pulse (intensity of about $3x10^{11}$ W/cm^2 and a pulse duration of roughly 30 fs), two-color two-photon transitions will be induced, yielding electrons with a kinetic energy between the harmonics, at the position of the so-called sidebands (SB, Figs. 1(a) and (b)). Within the framework of second order perturbation theory, only the two nearest harmonics of order 2q ± 1, with q an integer number, contribute to each sideband peak of order 2q. Quantum path interference will lead to an oscillation of the SB2q signal as a function of pump-probe delay that can be approximated by [11]:

$$SB_{2q}(t) \approx \cos\left(2\omega_{IR}t - \Delta\varphi_{XUV} - \Delta\varphi_{at}\right) \quad (1)$$

Optics EXPRESS

where t is the delay between the pump and the probe pulse, $\Delta\varphi_{XUV}$ represents the additional phase term acquired due to the chirp of the APT and $\Delta\varphi_{at}$ refers to the atomic scattering phase, which in terms of time delays becomes to:

$$\tau_{at} = \hbar\frac{\partial\varphi_{at}}{\partial E} \cong \hbar\frac{\Delta\varphi_{at}}{\Delta E} \tag{2a}$$

This time delay in the RABBITT techniques consists of a sum of two terms: the Wigner time delay τ_W and the continuum-continuum time delay τ_{CC} [4]. With τ_W we measure the group delay experienced by electron wave packet under the short-range influence of a Coulomb potential with respect to a free electron with the same kinetic energy [24]. The additional term τ_{CC}, on the other hand, is measurement-induced and is introduced in the additional quantum transition between two electronic states in the continuum with the IR probe pulse interaction [Fig. 1(a)] [25,26]. The total phase of each SB, $\Delta\varphi_{at}^{Ar/Ne}$, results then in the sum of two measurement-induced phases, $\Delta\varphi_{XUV}$ and $\Delta\varphi_{CC}$ (i.e. $\Delta\varphi_{CC} = 2\omega_{IR}\tau_{CC}$), and the Wigner phase $\Delta\varphi_W$ (referring to the Wigner time delay τ_W). When computing the difference between two SB phases of the same order 2q but from the two different gases under test, only the XUV phase, $\Delta\varphi_{XUV}$, cancels out. This means that the measured relative time delay represents the difference between the atomic delays of argon and neon:

$$\begin{aligned}\Delta\tau^{Ar-Ne} &= \hbar\frac{\partial}{\partial E}\left(\varphi_{at}^{Ar} - \varphi_{at}^{Ne}\right) \cong \hbar\frac{\Delta\varphi_{at}^{Ar} - \Delta\varphi_{at}^{Ne}}{\Delta E} = \\ &= \hbar\frac{\left(\Delta\varphi_{W}^{Ar} + \Delta\varphi_{cc}^{Ar}\right) - \left(\Delta\varphi_{W}^{Ne} + \Delta\varphi_{cc}^{Ne}\right)}{\Delta E}\end{aligned} \tag{2b}$$

2.1.1 Data analysis

Figure 2 shows the principle of the photoemission time delay extraction with the RABBITT technique. By measuring the time-of-flight of the ions in coincidence with the electrons we are able to record RABBITT traces of photoelectrons released from Ne 2p and Ar 3p simultaneously [Figs. 2(a) and 2(b)]. To extract the phase for each SB we integrate the signal within an energy range of 0.7 eV around the SB maximum as shown in Figs. 2(a) and 2(b) and then subtract the DC component, obtaining the blue dashed curve in Figs. 2(c) and 2(d). Then, we Fourier transform the curves to filter the signal at frequency $2\omega_{IR}$, as shown in Figs. 2(e) and 2(f) (red dashed curve). The obtained frequency-filtered SB signals (red solid curves in Figs. 2(c) and 2(d)) are subsequently fitted with the following equation:

$$f(t)_{SB_{2q}} = A_{2q}\cdot e^{\left(\frac{t-t_0}{\sigma}\right)^2}\cdot\cos\left(2\pi ft - \Delta\theta_{2q}\right) \tag{3}$$

where A_{2q}, t_0, σ and $\Delta\theta_{2q}$ are the fitting parameters while the value of the frequency $\omega = 2\omega_{IR}$ is extracted from the Fourier analysis of the raw data [Figs. 2(e) and (f)] and kept fixed during the fitting procedure. In particular, $\Delta\theta_{2q}$ is the SB phase we are interested in.

Optics EXPRESS

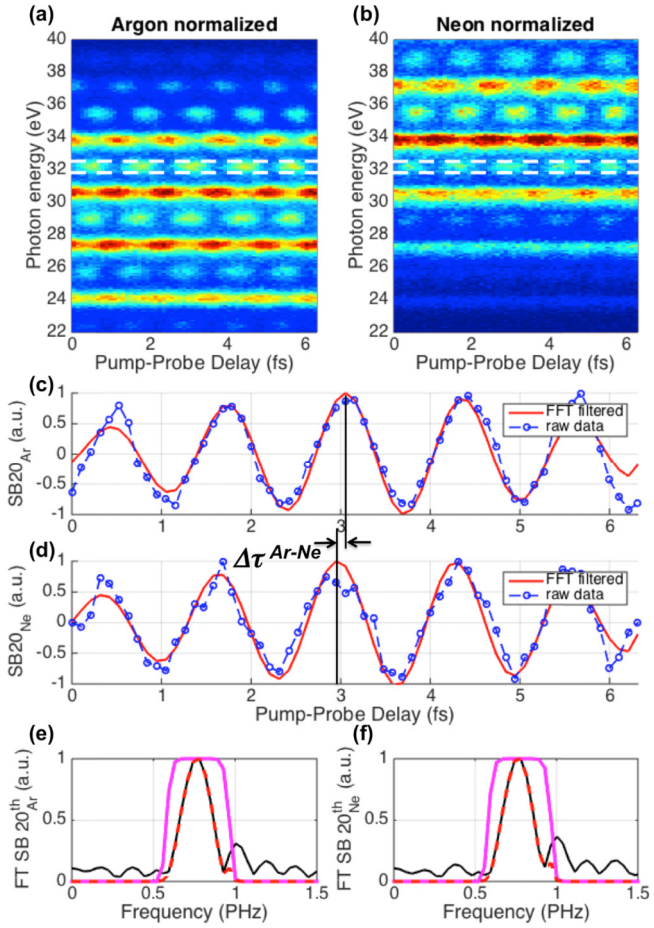

Fig. 2. RABBITT traces for Ar 3p (a) and Ne 2p (b) measured with an XUV-APT pump and an IR probe with a center wavelength of 772 nm. The blue circle dashed lines in (c) and (d) represent the photon-energy-integrated signals of SB 20 for Ar and Ne, corresponding to the highlighted areas in Fig. (a) and (b), minus their DC component, while the red solid lines represent the frequency-filtered SB phases. e) and f) show the Fourier transform (black solid line) of the raw SB signal (blue circle dashed lines in (c) and (d)), the frequency filter (magenta solid line) and the resulted frequency-filtered SB signal (red dashed line) as a function of the frequency expressed in PHz.

Within the finite difference approximation one can write:

$$\Delta\tau_{2q}^{Ar-Ne}(\omega) \cong \frac{\Delta\theta_{2q}^{Ar} - \Delta\theta_{2q}^{Ne}}{2\omega_{IR}} \tag{4}$$

with which one can directly obtain the relative atomic photoionization time delay corresponding to the SB order 2q.

2.2 Attosecond energy streaking

In attosecond energy streaking photoelectrons are generated from the target atom by the interaction with an XUV-SAP in the presence of a few-cycle near-infrared laser pulse with a stabilized carrier-envelope phase and linear polarization. The intensity of the IR pulse should be sufficiently low to leave the bound electrons unaffected, but high enough to significantly accelerate or decelerate the liberated electrons: i.e. to streak the EWP in the continuum. We

then map the time-dependence of the few-cycle IR field to the final electron energy after the IR pulse. Thus starting the liberated electron trajectories in the continuum at different times within the driving IR field will result in different final momenta. A streaking spectrogram is a set of photoelectron spectra, each shifted differently by the IR pulse as a function of XUV-IR delay [Fig. 1(d)]. In our experiments we use a SAP centered around 35 eV with a bandwidth of approximately 12 eV as a pump [Fig. 1(c), inset]. The waveform-controlled, intense few-cycle IR pulse was used as the probe pulse with a peak intensity of $3\text{x}10^{12}$ W/cm^2 and a pulse duration of 6 fs. Again, we used a COLTRIMS detector to simultaneously measure the streaking traces of the two species, Ar and Ne, assigning each detected photoelectron to its parent ion. Thus ensuring the same experimental conditions for both target gases.

2.2.1 Data analysis: FROG CRAB reconstruction

In order to extract any photoionization time-delay information from an attosecond streaking spectrogram we need to retrieve the amplitude and phase of the streaked EWP. The FROG-CRAB retrieval algorithm is most commonly used [19,27]. Within the strong-field approximation (SFA) the photoelectron spectrum can be written such that the corresponding expression mimics the definition of a FROG spectrogram [Eq. (5)a)], i.e. as the modulus square of the Fourier transform of the product of a 'pulse' function with a time delayed 'gate' function: pulse, $P(t-t_d)$, and gate, $G(t)$ [19,27,28]:

$$S_{FROG}(\omega,t_d)=\left|\int_{-\infty}^{+\infty}P(t-t_d)G(t)e^{i\omega t}\,dt\right|^2 \tag{5a}$$

$$S(\vec{p},t_d)=\left|\int_{-\infty}^{+\infty}E_{XUV}(t-t_d)d_{\vec{p}(t)}\cdot e^{-i\varphi(\vec{p},t)}e^{i(p^2/2+I_p)t}\,dt\right|^2 \tag{5b}$$

$$\varphi(\vec{p},t)=\int_{t}^{+\infty}dt'\left[\vec{p}\cdot\vec{A}_{IR}(t')+A_{IR}^2(t')/2\right] \tag{5c}$$

Equation (5b), expresses the streaking spectrogram where three main terms can be identified. The first one is the product $E_{XUV}(t-t_d)d_{\vec{p}(t)}$, which corresponds to the pulse $P(t-t_d)$ in Eq. (5a). This expression describes the XUV-pulse delayed by t_d with respect to the IR field multiplied by the dipole transition matrix element describing the transition from the ground state to the continuum. As a result of the SFA, the influence of the atomic Coulomb potential on the free electron is neglected. Therefore, the final continuum state is not an accurate scattering wavefunction, but a plane wave with instantaneous momentum $\vec{p}(t)=\vec{p}+\vec{A}_{IR}(t)$ where $\vec{p}(t)$ is the asymptotic momentum of the photoelectron and $\vec{A}_{IR}(t)$ is the vector potential of the IR field, $\vec{E}_{IR}(t)=-\dfrac{\partial\vec{A}_{IR}(t)}{\partial t}$. In this paper atomic units are always used unless otherwise stated. The second term in Eq. (5b), i.e., $e^{-i\varphi(\vec{p},t)}$, represents the gate $G(t)$ and is a pure phase term [Eq. (5c)] which modifies the trajectory of the EWP depending on its time of appearance within the optical field cycle. The final kinetic energy of the EWP $p^2/2$ and the ionization potential I_p are given in the last term. Due to the scalar product $p\cdot\vec{A}_{IR}(t')$ in Eq. (5c) the photoelectrons have to be observed along a given direction to define a common modulation phase (in our case we choose a cone between −30° and 30° with respect to the laser polarization). In order for the streaking spectrogram $S(\vec{p},t_d)$ [Eq. (5b)] to correspond to the definition of a FROG-spectrogram (Eq. (5a)), the pulse and the gate should not be functions of the electron final momentum $\vec{p}(t)$. This requirement can be easily

Optics EXPRESS

fulfilled by approximating p with the value of the center momentum of the unstreaked photoelectron spectrum, p_C. This means that the dipole transition matrix element is considered constant within the XUV bandwidth: $d_{\vec{p}(t)} = d_{p_C}$, and thus the gate becomes $e^{-i\varphi(p_C,t)}$. This approximation is known as the central momentum approximation (CMA).

After modifying the streaking trace to fit the mathematical structure of the general FROG Eq. (5a), multiple iterative algorithms are available for the retrieval of the spectral intensity and phase for the pulse and gate simultaneously. Simultaneous retrieval of pulse and gate is also known as blind-FROG [29]. In this work we choose the algorithm named Least-Squares Generalized Projections Algorithm (LSGPA) using square matrices as an input to perform all our reconstructions [30]. Generally, the experimental traces are rectangular matrices meaning that the energy sampling resolution is usually much higher than the number of sampled pump-probe delay points. In order to create square matrices, we need to perform an interpolation. We choose the same number of bins $N_t = 2^9$ and $N_\varepsilon = 2^9$ to interpolate the time and energy axis, respectively, in order to fulfill their Fourier relationship. As a result, the time step is 28.9 as and the energy step is 0.28 eV. The latter will define the sampling resolution of the reconstructed spectral phase and consequently the sampling resolution of $\Delta\tau_{Ar\text{-}Ne}(\omega)$. The Ar and Ne group delays are in fact the first derivative with respect to the energy of the spectral phases of the reconstructed EWP (the pulse function in Eq. (5a)), which can be expressed within the finite difference approximation as:

$$\frac{d\varphi(E)}{dE} = \frac{\varphi(E+\Delta E)-\varphi(E-\Delta E)}{2\Delta E} + O(\Delta E^2) \qquad (6)$$

where ΔE is the derivation step. While in the RABBITT case ΔE is intrinsically limited to $2\omega_{IR}$, in attosecond streaking ΔE can be chosen arbitrarily depending on Nε, limited only by the sampling grid.

We have an ambiguity of the "time-zero" in each FROG reconstruction. In order to guarantee the same "time-zero" in both Ar and Ne streaking traces, a possible option consists in "patching" the traces in a single matrix [5]. In this case the Ar trace is shifted by an arbitrarily chosen energy of 40 eV, in order to have one common energy axis and avoid spectral overlap between the two traces. After the reconstruction, the spectra and phases are disentangled at their patched energy, 40 eV, by shifting the Ar data back to its original spectral position [5]. In principle CMA can introduce a significant error because we artificially change the value of pc for the Ar trace during the patching procedure. However, it has been demonstrated that in case of a sufficiently narrow XUV-SAP bandwidth as used here [Fig. 1(c), inset], the introduced error is negligible [20].

In order to fulfill the CMA while maintaining the same time-zero for both Ar and Ne spectrograms we decided not to use the patching method, but to choose a different approach instead. We implemented a nested FROG-CRAB loop that reconstructs both the Ar and Ne streaking traces in parallel, starting from an identical initial guess for the pulse and gate. The algorithm runs for the two traces in parallel. Before starting a subsequent iteration, the new guess for the gate is set to the average of the two updated gates obtained from the individual Ar and Ne traces. In this way each iteration starts with a common gate and pulse pair for both traces and consistency between the two reconstructions is assured. To compare the "nested-loop method" with the "patching method", we simulated Ar and Ne traces using Eq. (5b) and (5c) [28]. The temporal EWP generated during a XUV photoionization process, i.e. the pulse in the FROG-spectrogram, can be described as the inverse Fourier transform of the product $\tilde{E}_{XUV}(\omega)d(\omega)$, where the first term is the Fourier transform of the XUV pulse and the second is the dipole transition matrix element which can be approximated as a pure phase term $e^{i\varphi_{at}(\omega)}$ [20]. In all our simulations we use the $\varphi_{at}(\omega)$ of Ar and Ne published by Kheifets in [31]. The theoretical curves were calculated using the random-phase-

Optics EXPRESS

approximation with exchange (RPAE) method considering screened dipole interactions which include the dynamical correlations among all electrons in the outermost occupied atomic orbital of Ar and Ne, which are the 3p and 2p orbitals, respectively, in an energy-range starting from 28 eV. As simulation parameters we use a transform limited SAP with a duration of 230 as and a center energy of 33 eV. For the IR field we considered a wavelength of 786 nm with a pulse duration of 5 fs and an intensity of $3x10^{12}$ W/cm^2. The pump-probe delay step was 0.05 fs. These parameters were selected to resemble the experimental conditions. As an example, Figs. 3(a)-3(d) show the simulated and reconstructed traces using the nested-loop method. The agreement between the input and output spectrograms is evident as well as for the extracted relative delays $\Delta\tau_{Ar\text{-}Ne}$ [Fig. 3(e)].

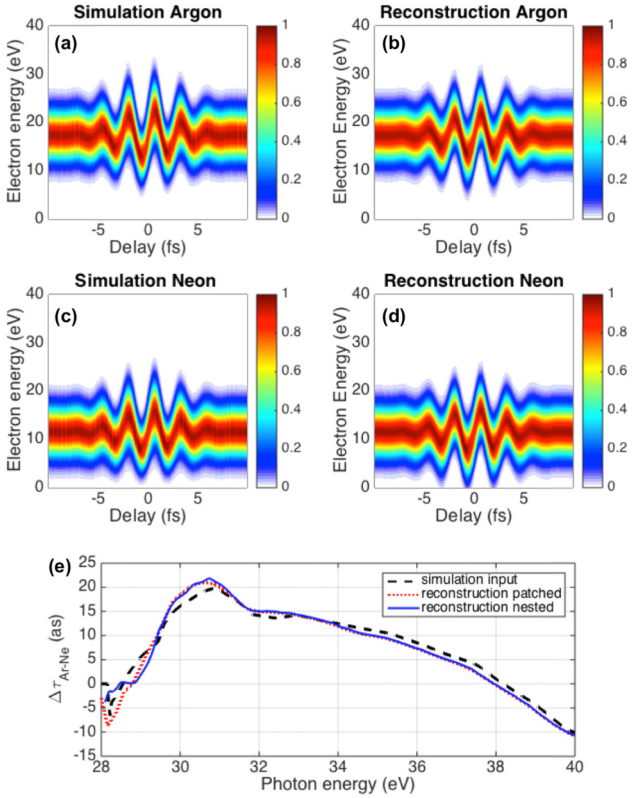

Fig. 3. LSGPA nested reconstruction algorithm. a) and c) show the simulated streaking traces of Ar and Ne, respectively; b) and d) show the reconstructed traces based on the nested-loop method. e) shows the relative Ar-Ne delay, $\Delta\tau_{Ar\text{-}Ne}$, for the nested-loop (blue solid curve) and patched (red dotted curve) reconstructed methods. The input is the dashed black curve.

2.3 Robustness against chirped XUV pulses

Recently, Wei and co-authors [20] critically investigated the reliability of the FROG-CRAB reconstruction when used to extract photoemission time delays. They claim that the spectrogram is only weakly sensitive to the small changes introduced by the dipole phase and if any major phase term is added, like the XUV phase of a chirped pulse, this will dominate in the reconstruction resulting in a wrongly retrieved dipole phase. Since the attosecond pulses used in a real experiment will always have a certain amount of residual chirp, the capability of streaking combined with the FROG-CRAB reconstruction method to retrieve small photoemission delays is questioned. In addition it is not clear if the RABBITT measurements are affected by the same problem. We focus in this section to a critical investigation of the

Optics EXPRESS

reliability of the retrieved time delays for both techniques, RABBITT and streaking, when used in combination with chirped XUV pulses.

We therefore performed new simulations adding three different values of chirp to the XUV pulse: such as 0, 0.01 and 0.02 fs^2. The last value is the closest to our experimental value, i.e. 0.0195 ± 0.006 fs^2. The simulation parameters for the streaking case are the same as discussed in the previous paragraph. For the RABBITT simulations, we used the same SFA equation used for streaking, i.e. Equation (5)a) and (5b) [16]. The wavelength of the IR field was tuned from 760 to 772 nm, with a pulse length of 30 fs and intensity $I_{IR} = 1x10^{11}$ W/cm^2. The XUV pulse train has an envelope centered at 32.9 eV (772 nm) to 33.4 eV (760 nm), with a duration of 350 as for the individual pulses in the train. The parameters were chosen to best match the experimental conditions. The pump-probe delay step was chosen to be equal to 0.1 fs.

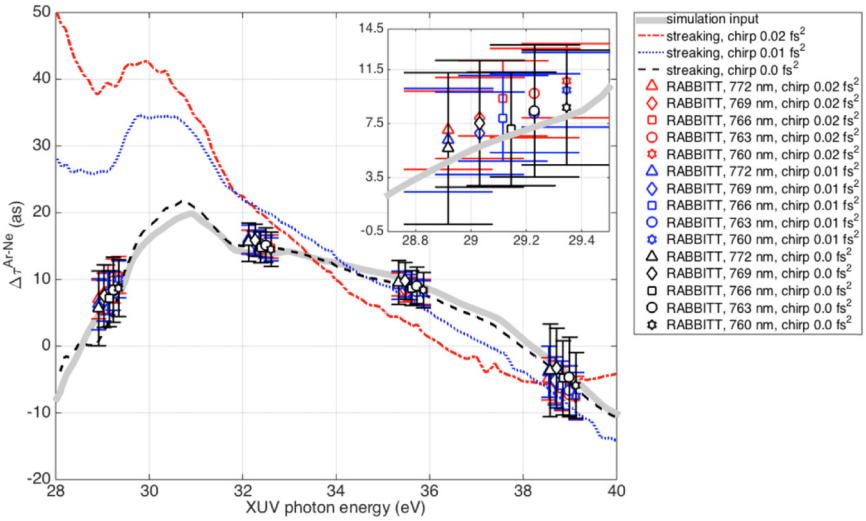

Fig. 4. Simulation experiments for a given input delay (grey solid curve): Difference in group delay between Ar and Ne retrieved by FROG-CRAB from simulated streaking traces (dashed curves) and RABBITT traces (scattered data points with different shapes corresponding to different IR wavelengths) using the same input delay but using different XUV chirp values with a GDD of 0 fs^2, 0.01 fs^2 and 0.02 fs^2 (black, blue and red).

Figure 4 shows the atomic time delay difference $\Delta\tau_{Ar\text{-}Ne}$ as a function of the XUV photon energy extracted from simulated streaking and RABBITT traces for a given input delay (Fig. 4, grey solid line) and for different XUV chirp values (i.e. GDD of 0 fs^2 in black, 0.01 fs^2 in blue and 0.02 fs^2 in red). The error bars for the RABBITT case represents the 95% confidence intervals form the sidebands fit. As observed by Wei and associates [20], it is evident how the resulting time delays from the streaking reconstruction exhibit a reconstruction error that increases with an increasing chirp in the XUV pulses (Fig. 4 dashed curves), whereas the RABBITT delays are clearly not affected (Fig. 4, data points with different colors overlap within the error bars). This may appear quite surprising considering that a RABBITT spectrogram can be constructed from the interference of several streaking spectrograms [17], meaning that one would expect to maintain the same dependence on the XUV-chirp. In [20], Wei et al. attribute the dependence of the streaking results on the XUV-chirp to the poor sensitivity of the streaking spectrogram to small variations of the EWP phase. Combining the explanation reported in [20] with our results, one would then come to the puzzling conclusion that a RABBITT spectrogram is more sensitive than a streaking spectrogram to small values of the atomic phase.

Optics EXPRESS

In order to investigate the origin of the discrepancy between RABBITT and streaking results, we decided to look more closely at the role of the CMA in the reconstruction procedure. The FROG-CRAB algorithm is, in fact, based on the CMA, whereas this approximation is not needed in the RABBITT analysis. The CMA is quite a strong approximation that might lead to an additional reconstruction error in the case of a chirped XUV pulse.

In order to verify this "CMA-error" hypothesis we simulate streaking traces for Ar and Ne using differently chirped XUV pulses. For each simulation we substitute the final electron momentum $p(t)$ [Eq. (5b) and (5c)] with the center momentum of the unstreaked photoelectron spectrum p_C, forcing the simulated streaking trace to be compatible with the CMA, i.e. to be a FROG spectrogram [Eq. (5a)].

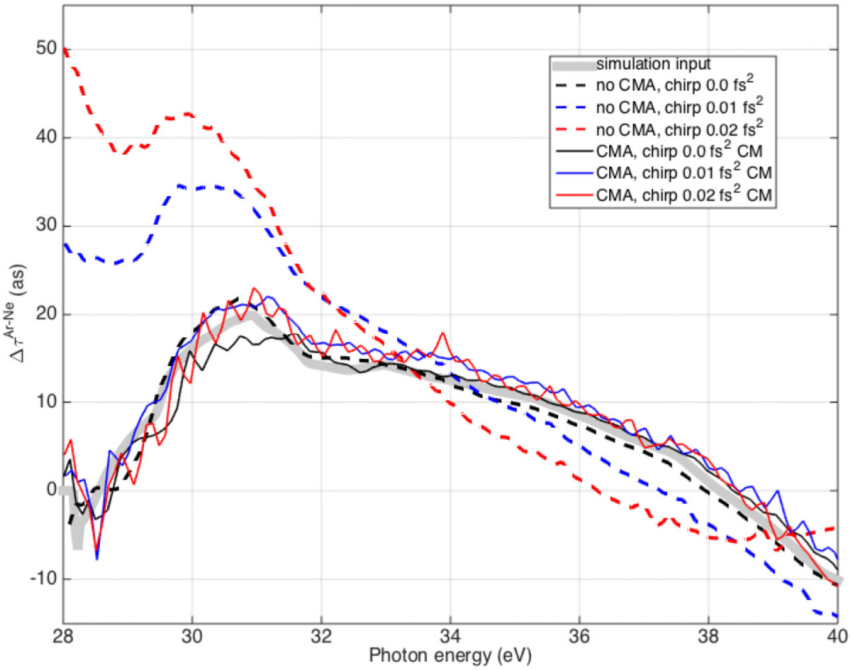

Fig. 5. Simulation experiments testing the "CMA-error" hypothesis: FROG-CRAB retrieved group delay differences between Ar and Ne from simulated streaking traces with (solid) and without (dashed) the CMA for different chirp values: 0 fs^2 (black), 0.01 fs^2 (blue) and 0.02 fs^2 (red). The simulation input is the grey solid curve.

Figure 5 shows the comparison between $\Delta\tau_{Ar-Ne}$ reconstructed from streaking traces simulated with and without the CMA. The delays retrieved from the simulations based on the CMA do not show any dependence on the XUV chirp and are in perfect agreement with the initial theoretical input. In contrast to the conclusion of Ref [20]. we find that the FROG-CRAB reconstruction outcome is very sensitive to any deviation from the CMA. For chirped XUV pulses the difference between applying or ignoring the CMA becomes more significant [Fig. 6]. For an easier comparison, Figs. 6(e) and 6(f) show the difference of the spectrograms simulated with and without the CMA for XUV-chirp values of 0 and 0.02 fs^2. We can divide the streaking trace into two temporal regions: (1) pump-probe overlap around the zero time delay and (2) large time delays where the photoelectron spectrum is not affected by the IR pulse. As one can observe in Fig. 6(f), by applying the CMA with chirped pulses we introduce an appreciable error also in region (2). This translates into a more pronounced difference between the unperturbed photoelectron spectrum at big delays and the streaked photoelectron spectrum at the temporal overlap, which is interpreted by the reconstruction

Optics EXPRESS

algorithm as a stronger effective XUV-chirp and therefore leads to the false reconstruction of the photoelectron spectral phase (see Fig. 5 dashed curves). This effect is not present in the case of transform-limited attosecond pulses (see the solid curves in Fig. 5 and the region (2) in Fig. 6(e)).

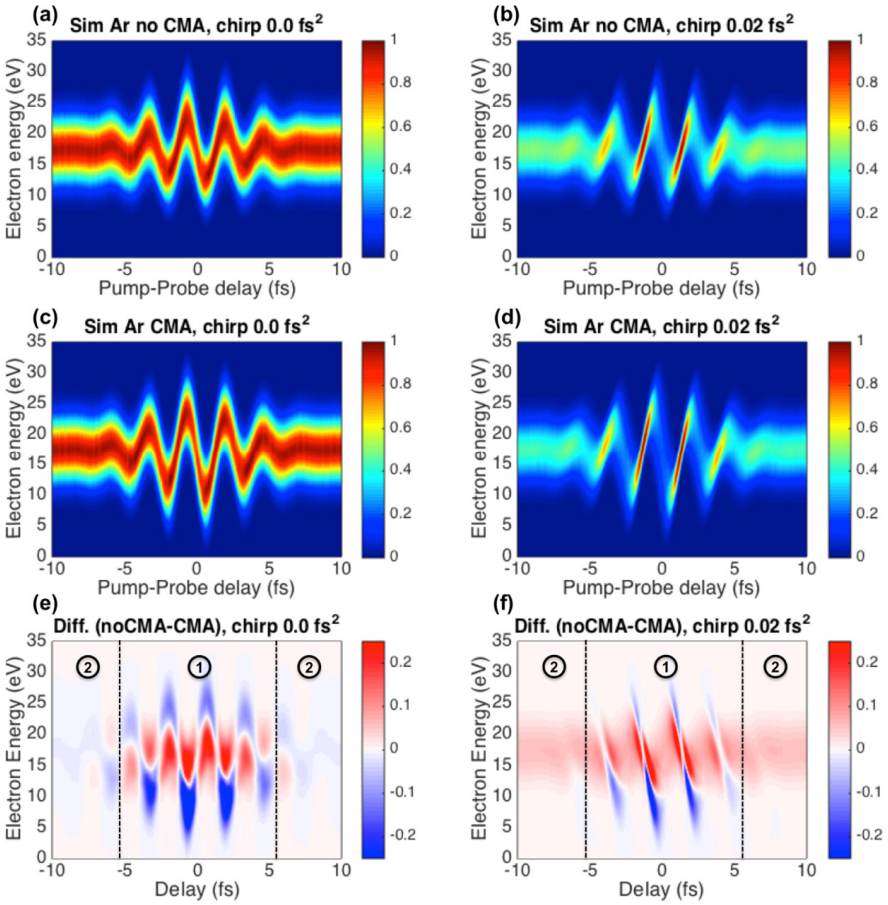

Fig. 6. Simulated Ar streaking traces for an unchirped XUV pulse (a and c) and with an XUV chirp of 0.02 fs^2 (b and d) with (c and d) and without (a and b) applying the CMA. As one can observe, a main effect of the CMA is that the streaking amplitude towards low energies becomes the same as towards high energies. This effect is displayed in e) and f) which represent the spectrogram difference a) - c) and b) - d), respectively. Two temporal regions are emphasized by the dashed black lines and numbers: region (1) is the time zero XUV-IR overlap while region (2) indicates large pump-probe delays at which there is almost no interaction between the two fields.

3. Discussion

We observed that the RABBITT data analysis is very robust with regards to a possible XUV chirp. In contrast the streaking data analysis shows a severe systematic error as the XUV-chirp increases, due to the deviations from the CMA on which the FROG-CRAB algorithm is based.

On the other hand the RABBITT technique only provides a measured delay at coarsely sampled energy points separated by $2\omega_{IR}$, whereas the streaking technique gives a retrieved $\Delta\tau_{Ar\text{-}Ne}$ with very fine energy sampling resolution.

Optics EXPRESS

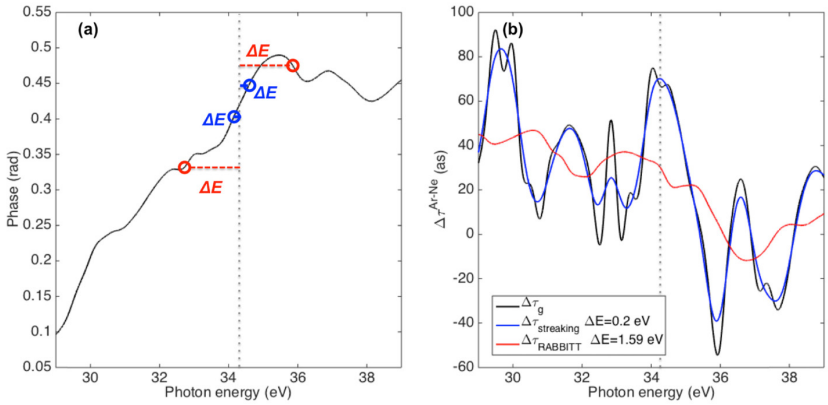

Fig. 7. Comparison between RABBITT-like and streaking-like sampling when assuming a moderately fast oscillating dipole phase: (a) represents the input phase [32], while (b) reports the first derivative of this phase in the finite difference approximation according to the RABBITT-like [Eq. (4)] and streaking-like [Eq. (6)] definitions obtaining the red and blue curves, respectively. The correct delay curve corresponding to the given phase is shown in black. The red and blue arrows in (a) display graphically the different sampling performed by the finite differentiation done for the case of RABBITT (red arrows) and streaking (blue arrows).

The coarse sampling resolution in RABBITT clearly affects its ability to correctly sample fast varying dipole phases such as we would expect in the presence of resonances. In case of streaking the reconstruction should provide enough energy resolution to overcome this limit. This can be observed in Fig. 7(b) where the input delay (black curve) results from the first derivation of the Ar dipole phase used by Carette et al. [32] shown in Fig. 7(a). The blue curve [Fig. 7(b)] corresponds to a streaking-like derivation [Eq. (6)] with a ΔE of 0.2 eV as shown with blue arrows and circles in Fig. 7(a). The streaking reconstruction is able to follow the main features of the input delay (black curve). The red curve corresponds to a RABBITT-like finite-difference derivation [Eq. (4)] with a much larger ΔE of 1.59 eV shown with red arrows and circles in Fig. 7(a), corresponding to λ_{IR} = 780 nm. In this case the RABBITT reconstruction results in a smoothed version of the exact delay. This means that RABBITT will always fail in retrieving variations of the dipole phase with energy that change fast compared to its intrinsic sampling resolution of $2\omega_{IR}$.

Recently alternative solutions to overcome this RABBITT energy sampling limitation have been demonstrated by using for example longer IR probe wavelengths to have a finer energy sampling [33], or tuning the IR probe wavelength to shift the resulting XUV spectrum in energy and move a specific HH order across a resonance [34]. Only in this condition the sidebands adjacent to this HH will present a modulation in their phase due to the interaction with the resonance. Moreover, Gruson et al [35], has demonstrated the possibility to perform in each sideband a spectrally-resolved analysis retrieving the phase modulation over about 700 meV.

Keeping this in mind we can now analyze the actual experimental traces and compare the obtained results. Figure 8 shows the comparison between the experimental $\Delta\tau_{Ar-Ne}$ obtained from the two techniques. The streaking curve (blue, solid line) is the average of 17 independent measurements (Ar and Ne simultaneously measured) affected by a chirp of about 0.02 fs^2. The shaded blue region represents the standard deviation of these 17 measurements (each reconstruction was performed using the LSGPA algorithm, $N_\varepsilon = N_\tau = 29$ and 5000 iterations). To increase the energy coverage of the sampling points from the RABBITT measurements, we tuned the center IR wavelength to three different values: 772, 765 and 760 nm and extract the relative $\Delta\tau_{Ar-Ne}$. Each RABBITT spectrogram is measured by integrating the photoelectron spectrum for 100 s (10 kHz laser repetition rate) at each pump-probe delay,

Optics EXPRESS

with delay points separated by about 0.1 fs. Each RABBITT data point in Fig. 8 represents the statistical variation over a set of independent measurements (weighted mean) taking into account the additional uncertainty resulting from the fitting-procedure [Eq. (3)] to extract the SBs phase term as follows:

$$\overline{x}_w = \frac{\sum_{i=1}^{N} \frac{x_i}{\sigma_i^2}}{\sum_{i=1}^{N} \frac{1}{\sigma_i^2}} \tag{7}$$

where x_i represents each single measurements, N is the total number of measurements, $1/\sigma_i^2$ is the weight and σ_i is the standard deviation resulting from each SB-fit, considering a 95% confidence interval (σ_i = 1.96∗conf. int.). Moreover, the presented errorbars include two terms, one is the weighted estimator of the variance of each measurements x_i with respect to the calculated mean value $\overline{x}$, and one is the weighted mean of σ_i calculated as follows with Eq. (7):

$$\delta x_{tot} = \sqrt{\delta x_w^2 + \delta\sigma_w^2} = \sqrt{\frac{N\sum_{i=1}^{N} \frac{\left(x_i - \overline{x}_w\right)^2}{\sigma_i^2}}{(N-1)\sum_{i=1}^{N} \frac{1}{\sigma_i^2}} + \left(\frac{\sum_{i=1}^{N} \frac{1}{\sigma_i}}{\sum_{i=1}^{N} \frac{1}{\sigma_i^2}}\right)^2} \tag{8}$$

For the sake of comparison, we also report the experimental results of the $\Delta\tau_{Ar\text{-}Ne}$ from Guenot et al. [14] (dark green squares) measured with the RABBITT technique. These independent measurements are in good agreement with our data.

Optics EXPRESS

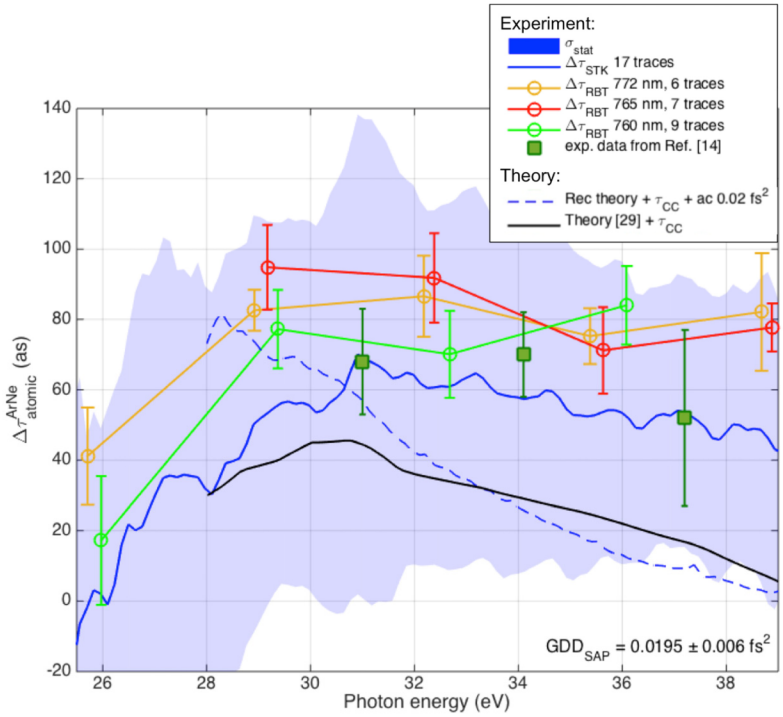

Fig. 8. Comparison between experiments and theory: average difference in group delay between Ar and Ne as retrieved by FROG-CRAB from experimental streaking traces (blue solid curve) and by RABBITT (colored symbols) compared to the theoretical prediction (solid black curve). Additionally, the reconstructed difference in Ar-Ne group delay from the simulated streaking trace with an XUV attochirp of 0.02 fs^2 (dashed blue curve), and the experimental data points (dark green scattered squares) published in [14] are shown. Our averaged experimental chirp retrieved by the FROG-CRAB algorithm is 0.0195 ± 0.006 fs^2. The experimental delay difference shown for the streaking method is the result of the average of 17 independent measurements and the blue shaded area is the relative standard deviation. In case of the RABBITT data, the average has been weighted considering the standard deviation σi of the fit function [Eq. (7)] and corresponding weighted errorbars [Eq. (8)]. The 772-nm data points are the results from an average of 6 traces (yellow circles), the 765-nm data was averaged over 7 traces (red circles) and the 760-nm data over 9 traces (light green circles).

The experimental data are also compared with the theoretical prediction used for the simulations (solid black) and the reconstructed phase from the simulated streaking traces with the chirp close to the experimental value (dashed blue) [31]. These two curves are plotted for comparison with the experimental streaking time delays that are altered by the presence of a chirped XUV pulse. The delays extracted using the FROG-CRAB algorithm at XUV-energies below about 33 eV appear to be overestimated while those at higher XUV-energies are underestimated. If we take this into account, the experimentally determined streaking and RABBITT time delays become more similar, leading to the conclusion that both techniques measure the same photoemission time delays.

On the other hand, a visible disagreement between the theory and the overall experimental results remains. Moreover, it is well known that photoionization dynamics can be strongly affected by the presence of resonances. Ar in particular presents a significant number of resonances in the range between 25 and 30 eV [32]. For example, Kotur et al. recently demonstrated the possibility to measure the phase distortion induced by the coupling between the continuum and an Ar autoionizing state located at 26.6 eV using the RABBITT technique [34]. The fact that we do not observe any evidence of such resonances in our experimental results is because our APT-XUV spectrum is not resonant with any of the resonances in the

Optics EXPRESS

range 25-30 eV. It is worth pointing out that the IR pulses used in the streaking experiment are usually ten times stronger than the ones used in the RABBITT experiment. Therefore, in the case of streaking, the IR can significantly alter the lifetime of the resonances and therefore the associated time delays.

4. Conclusion

In this work we critically investigated the two main techniques, RABBITT and attosecond energy streaking, currently used to extract electron dynamics from many different systems ranging from noble gases to condensed matter, and compare their experimental results. In particular we analyzed the reliability of the data-processing methods used to extract newly measured photoemission time delays between electrons released from the Ne 2p and Ar 3p ground states. We observed that both techniques lead to very similar results if we take into account that the obtained atomic delays suffer from different experimental-analysis conditions: the RABBITT technique, in fact, appears to be more robust against the presence of chirped XUV pulses but it has an intrinsic limitation through its coarse energy-sampling resolution that is fixed at $2\omega_{IR}$. Moreover, in case of fast varying dipole phases, e.g. in the vicinity of resonances, the photoemission delay will not be sampled correctly and the smoothed finite-difference derivative obtained with RABBITT will wash out any fast varying contribution.

On the other hand, attosecond streaking requires a reconstruction process that is highly influenced by the presence of a chirp on the XUV pulse. In fact, the chirp modifies the spectrogram features in such a way that the FROG-CRAB algorithm based on the CMA cannot correctly reconstruct, resulting in a wrong retrieved spectral phase. In 2010 Chini et al. [36] proposed a different retrieval algorithm called PROOF based on the analysis of only two-photon interference transitions occurring when a continuous XUV spectrum and a dressing IR pulse are present. The PROOF limitations are the requirement of a relatively weak and long IR pulse, no simultaneous retrieval of both XUV and IR pulses, and no access to the transition matrix elements. Most recently, Keathley et al. [37] published a more promising algorithm based on a least square minimization approach without the use of Fourier transforms in the retrieval process. This means that the full mathematical structure of the SFA [Eq. (5a)] can be applied without CMA and interpolation in the energy domain to satisfy Fourier transform constraints. We therefore can expect in the future to continue to make progress in attosecond streaking measurement techniques.

Funding

European Reasearch Council (ERC) advanced grant ERC-2012-ADG_20120216 and NCCR MUST, funded by the Swiss National Science Foundation (SNSF).